JOURNAL OF GEOPHYSICAL RESEARCH, VOL. 103, NO. C9, PAGES 18,851–18,866, AUGUST 15, 1998

Imaging of biogenic and anthropogenic ocean surface films by the multifrequency/multipolarization SIR-C/X-SAR

Martin Gade and Werner Alpers
Institut für Meereskunde, Universität Hamburg, Hamburg, Germany

Heinrich Hühnerfuss
Institut für Organische Chemie, Universität Hamburg, Hamburg, Germany

Harunobu Masuko and Tatsuharu Kobayashi
Communication Research Laboratory, Tokyo, Japan

Abstract. Results from the analyses of several spaceborne imaging radar-C/X-band synthetic aperture radar (SIR-C/X-SAR) images are presented, which were acquired during the two SIR-C/X-SAR missions in April and October 1994 by the L-, C-, and X-band multipolarization SAR aboard the space shuttle Endeavour. The images showing natural (biogenic) surface slicks as well as man-made (anthropogenic) mineral oil spills were analyzed with the aim to study whether or not active radar techniques can be applied to discriminating between these two kinds of surface films. Controlled slick experiments were carried out during both shuttle missions in the German Bight of the North Sea as well as in the northern part of the Sea of Japan and the Kuroshio Stream region, where surface films of different viscoelastic properties were deployed within the swath of the shuttle radars. The results show that the damping behavior of the same substance is strongly dependent on wind speed. At high wind speed (8–12 m/s) the ratio of the radar backscatter from a slick-free and a slick-covered water surface (damping ratio) is smaller than at low to moderate wind speeds (4–7 m/s). At 12 m/s, only slight differences in the damping behavior of different substances were measured by SIR-C/X-SAR. Furthermore, several SAR scenes from various parts of the world's oceans showing radar signatures of biogenic as well as anthropogenic surface films at low to moderate wind speeds are analyzed. The damping behavior of these different kinds of oceanic surface films varies particularly at L band where the biogenic surface films exhibit larger damping characteristics. Results of polarimetric studies from multipolarization SAR images showing various surface films are presented. It can be delineated from these results that Bragg scattering as well as specular reflection contribute to the backscattered radar signal at low incidence angles (up to 30°). It is concluded that at low to moderate wind speeds, multifrequency radar techniques seem to be capable of discriminating between the different surface films, whereas at high wind conditions a discrimination seems to be difficult.

1. Introduction

It is obvious that an effective oil spill surveillance, particularly of coastal waters, is necessary to avoid oil pollution of these sensitive sea areas or, more realistically, to keep it as small as possible. Oil films floating on the sea surface dampen the small surface waves [*Alpers and Hühnerfuss*, 1988, and references therein]. Since these waves are responsible for the backscattering of microwaves of comparable wavelengths (Bragg scattering, see *Valenzuela* [1978]), oil spills are visible as dark patches on radar images of the ocean surface. Further advantages of the use of radar techniques are that the microwaves are mostly not influenced by clouds and that active microwave techniques are independent of daylight. For these reasons the 5.3 GHz (C-band) synthetic aperture radar (SAR) aboard the first and second European Remote Sensing Satellites (ERS-1/2) is already used for operational oil surveillance (reported, e.g., by *Wahl et al.* [1994] and by *Pellemans et al.* [1995]).

However, not only anthropogenic surface films consisting of mineral oil dampen the surface waves and can be delineated on SAR images. Also, biogenic surface slicks, which are produced, e.g., by plankton and animals in the ocean [*Dietz and Lafond*, 1950; *Ewing*, 1950; *Hühnerfuss and Garrett*, 1981; *Alpers and Hühnerfuss*, 1989; *Lombardini et al.*, 1989], show strong wave-damping capabilities and thus can cause similar dark signatures in the SAR images, particularly when the radar operates at one single frequency (like the ERS-1/2). In order to reduce the risk of false alarms for the oil surveillance, *Wahl et al.* [1994], *Pellemans et al.* [1995], and *Sloggett and Jory* [1995] developed computer-based automated slick detection algorithms.

Biogenic surface slicks, because of their amphibilic molecular structure, form monomolecular surface films

Paper number 97JC01915.
0148-0227/98/97JC-01915$09.00

[*Hühnerfuss,* 1986]; that is, the thickness of the surface-active substance is very small in comparison to that of mineral oil spills. Therefore the viscoelastic properties of these surface films are different from the viscoelastic properties of oil spills, which in turn leads to a different damping of the ocean surface waves, the so-called Marangoni damping [*Lucassen-Reynders and Lucassen,* 1969; *Hühnerfuss,* 1986]. Following Marangoni damping theory, monomolecular surface films exhibit a resonance-like damping behavior, whereas the certain damping maximum is missing for (thick) mineral oil spills. In order to investigate the specific damping behavior of surface-active substances several experiments have been performed with natural and artificial sea slicks on the open ocean [*Garrett,* 1967; *Hühnerfuss et al.,* 1983a, b, 1994, 1996; *Ermakov et al.,* 1986; *Wu,* 1989; *Wei and Wu,* 1992; *Frysinger et al.,* 1992; *Onstott and Rufenach,* 1992] and in laboratory wind-wave tank facilities [*Lange and Hühnerfuss,* 1978, 1984; *Cini and Lombardini,* 1978; *Feindt,* 1985; *Hühnerfuss,* 1986; *Tang and Wu,* 1992; *Gade et al.,* 1998a]. In the latter instance it was shown that Marangoni damping [*Lucassen-Reynders and Lucassen,* 1969; *Cini and Lombardini,* 1978; *Alpers and Hühnerfuss,* 1989] is the dominant mechanism for the damping of short gravity sinusoidal waves by monomolecular slicks [*Hühnerfuss,* 1986]. However, because of the action of wind, additional energy fluxes also have to be taken into account.

The application of multifrequency radar techniques should therefore provide more reliable information about the viscoelastic properties and thus about the origin of the detected surface films. During the two spaceborne imaging radar-C/X-band synthetic aperture radar (SIR-C/X-SAR) missions in April and October 1994, called Space Radar Laboratory (SRL) 1 and SRL 2, a three-frequency/multipolarization SAR was flown aboard the space shuttle *Endeavour.* Several SAR images of the ocean surface, particularly of film-covered water surfaces, were acquired by SIR-C/X-SAR. In order to get a reliable set of reference data for the measured damping ratios, surface film experiments were carried out in the German Bight of the North Sea: during both shuttle missions, surface films of different viscoelastic properties were deployed within the shuttle swaths. Similarly, a certain quasi-biogenic substance (oleyl alcohol) was deployed on the water surface in the northern part of the Sea of Japan as well as in the Kuroshio Stream region south of Japan on several days during both shuttle missions in order to simulate natural surface slicks under different environmental conditions.

In this paper the results of these field experiments are presented and are compared with damping ratios derived from several SIR-C/X-SAR images of biogenic and anthropogenic surface films at different places of the world's oceans. A more detailed analysis can be found in work by *Gade* [1996].

2. Theoretical Background

During the experiments reported herein, measurements of the radar backscattering were performed at intermediate incidence angles (between 20° and 75°). For these incidence angles the radar backscattering from the water surface can be described to first order by Bragg scattering theory [*Wright,* 1968; *Valenzuela,* 1978]. According to this theory the normalized radar cross section (NRCS) is proportional to the spectral energy density of the Bragg waves, i.e., of those surface waves of wavelengths λ_B that obey the Bragg resonance condition

$$\lambda_B = \frac{\lambda_0}{2 \sin \vartheta} \quad , \tag{1}$$

where λ_0 denotes the radar wavelength and ϑ denotes the incidence angle. For a slick-free water surface the NRCS σ_0 can therefore be written as

$$\sigma_0 \;=\; T_{ij}\, \Psi(k_B)\,, \tag{2}$$

with

$$T_{ij} \;=\; \left|g_{ij}\right|^2 16\pi k_0^4 \cos^4 \vartheta\,,$$

where k_0 is the radar wavenumber. $\Psi(k_B)$ is the spectral power density of the Bragg waves with wavenumber $k_B = 2\pi/\lambda_B$. The function $|g_{ij}|^2$ depends on radar wavenumber, dielectric constant ε of the water, incidence angle, and polarization (ij = HH, VV, HV, and VH; H and V mean horizontal and vertical polarization, respectively. The first letter denotes the polarization of the transmitted radiation and the second letter denotes that of the received radiation). The thickness of a surface film (either a monomolecular slick or a thin oil spill) is small compared with the penetration depth of microwaves into the water; therefore we may assume that the Bragg coefficient T_{ij} is not affected by the presence of a thin surface film, i.e.,

$$T_{ij}^{(0)} \;\approx\; T_{ij}^{(s)}\,, \tag{3}$$

where the superscripts (0) and (s) denote a film-free and a film-covered water surface, respectively. It can be inferred from (2) and (3) that the polarization ratio, i.e., the ratio of the radar backscatter at horizontal and vertical polarization, is independent of a coverage of the water surface with a slick and can be written as:

$$\left(\frac{\sigma_{\mathrm{HH}}}{\sigma_{\mathrm{VV}}}\right)^{(0)} = \left(\frac{\sigma_{\mathrm{HH}}}{\sigma_{\mathrm{VV}}}\right)^{(s)} = \frac{T_{\mathrm{HH}}}{T_{\mathrm{VV}}} = \frac{\left|g_{\mathrm{HH}}\right|^2}{\left|g_{\mathrm{VV}}\right|^2}\,. \tag{4}$$

For an explicit expression of this ratio the reader is referred to *Valenzuela* [1978], for example.

The damping of small gravity and gravity-capillary water waves by monomolecular surface films can be explained by Marangoni damping theory [*Cini and Lombardini,* 1978; *Lucassen,* 1982; *Cini et al.,* 1983; *Alpers and Hühnerfuss,* 1989]. According to this theory the damping ratio $y(f)$, i.e., the ratio of the viscous damping coefficients $\Delta^{(s)}$ for a slick-covered and $\Delta^{(0)}$ for a slick-free water surface, can be approximated by the following expression:

$$y(f) = \frac{\Delta^{(s)}(f)}{\Delta^{(0)}(f)} = \frac{1 + X(\cos\theta - \sin\theta) + XY - Y\sin\theta}{1 + 2X(\cos\theta - \sin\theta) + 2X^2}\,, \tag{5}$$

where

$$X = \frac{|E|\,k^2}{\sqrt{2\omega^3 \eta \rho}} \qquad Y = \frac{|E|\,k}{4\eta\omega}\,.$$

Here $|E|$ and θ denote the absolute value and the phase of the complex dilational modulus $E = |E| \exp(i\theta - \pi)$ of the surface film, respectively, k is the wavenumber, and $\omega = 2\pi f = (g\,k + \tau k^3)^{1/2}$ is the angular frequency of the water surface waves. Here η and ρ are the dynamic viscosity and the density of the water, respectively, τ is the ratio of the water surface

Table 1. Absolute Values and Phases of the Dilational Modulus $E = |E| \exp(i\theta - \pi)$ for the Artificial Biogenic Substances Deployed in the Dedicated Field Experiments

Abbreviation	Substance	$\|E\|$, Nm^{-1}	θ, deg
OLA	oleyl alcohol	0.0255	-175
OLME	oleic acid methyl ester	0.0100	-5
TOLG	triolein	0.0115	-175

Compare Figure 1.

tension and density, and g is the acceleration of gravity. The rheological parameters $|E|$ and θ of the deployed substances were taken from *Hühnerfuss* [1986] and are summarized in Table 1. Inserting these parameters into (5) and setting $\tau = 7.3 \times 10^{-5} m^3/s^2$, $g = 9.81$ m/s^2, $\rho = 1000$ kg/m^3, and $\eta = 0.001$ Pa s, the theoretical damping curves shown in Figure 1 were calculated.

During both SIR-C/X-SAR missions in 1994, controlled surface film experiments were carried out. One of the goals of these experiments was to investigate the influence of environmental conditions (particularly of the wind speed) on the measured damping characteristic of the same substance (oleyl alcohol, OLA). From recent radar backscatter measurements with an airborne scatterometer [*Hühnerfuss et al.*, 1996; *Gade et al.*, 1998b; *Wismann et al.*, 1998; Wismann et al., The damping of short gravity-capillary waves by monomolecular sea slicks measured by airborne multi-frequency radars, submitted to International Journal of Remote Sensing, 1998 (hereinafter referred to as Wismann et al., submitted manuscript, 1998)] it was shown that no distinct damping maximum (as predicted by pure Marangoni damping theory) is measurable for OLA and that the damping behavior of this substance strongly depends on wind speed. In order to explain these observations one has to take into account the source terms of the action balance equation [*Hasselmann*, 1960],

$$0 = \frac{dN}{dt} = S_{wi} + S_{nl} - S_{vd} - S_{br}, \qquad (6)$$

where $N = \omega/k\Psi$ is the spectral action density of the water surface waves, and S_{wi}, S_{nl}, S_{vd}, and S_{br} are the source terms of

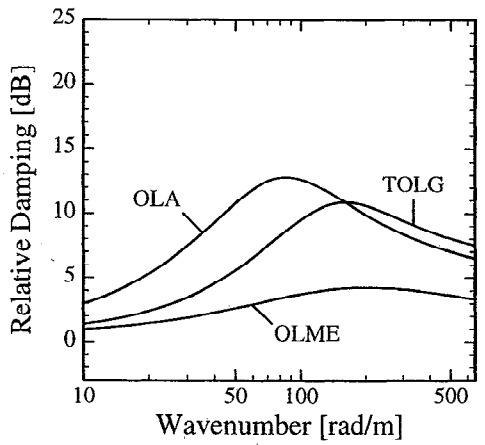

Figure 1. Theoretical damping curves for the deployed substances according to Marangoni damping theory; the parameters of the dilational modulus $E = |E| \exp(i\theta - \pi)$ are given in Table 1.

energy input by the wind, by nonlinear wave-wave interaction, and of energy loss by viscous dissipation and wave breaking, respectively. Expressions for the source terms of viscous dissipation and wind input can be found, e.g., in work by *Plant* [1982], *Mitsuyasu and Honda* [1982], *Phillips* [1985], and *Alpers and Hühnerfuss* [1989] as

$$S_{vd}^{(i)} = 2\Delta^{(i)} c_g N_i(k) \qquad (7)$$

$$S_{wi}^{(i)} = \beta^{(i)} N_i(k), \qquad (8)$$

where c_g is the group velocity of the water waves and $i \in \{0;s\}$. The function β depends on the angle between the wind and wave direction, the group velocity, and on the wind friction velocity. Using (2), (6), (7), and (8), one obtains for the theoretical damping ratio, i.e., the ratio of the (normalized) radar cross section of a slick-free and a slick-covered water surface

$$\frac{\sigma^{(0)}}{\sigma^{(s)}} = \frac{\Psi_0(k)}{\Psi_s(k)} = \frac{N_0(k)}{N_s(k)} = \frac{\beta^{(s)} - 2\Delta^{(s)} c_g}{\beta^{(0)} - 2\Delta^{(0)} c_g} \frac{S_{nl}^{(0)} - S_{br}^{(0)}}{S_{nl}^{(s)} - S_{br}^{(s)}} \cdot (9)$$

One certainly cannot assume that the water surface of the North Sea (or any other sea surface) is absolutely slick-free (compare the superscript (0) in (9)). However, to first order, we may assume that (9) gives a reasonable measure of the damping ratios. In order to use a simple notation we will hereinafter refer to the sea surface as "slick covered" or "slick free," corresponding to the film-covered water surface and the surrounding area, respectively.

The terms in the far right factor of (9), i.e., the source terms for nonlinear wave-wave interaction and for wave breaking, are still poorly known and cannot easily be determined. Recently, *Gade* [1996] showed that under high wind conditions (> 10 m/s) the reduction of the backscattered radar signal by different oceanic surface films measured by an airborne scatterometer can successfully be simulated using (9) by also taking the source terms for wave breaking into account. These results, however, are presented in another paper [*Gade et al.*, 1998b]. Particularly, under low to moderate wind conditions, where the energy input by the wind is too low to overcome the strong viscous dissipation by the slick, nonlinear wave-wave interaction plays an important role. Therefore we refrained from calculating theoretical damping ratios, however, (9) seems to be adequate for some qualitative analyses presented in this paper.

3. Experimental Results

Natural sea slicks have already been analyzed, e.g., by *Dietz and Lafond* [1950], *Ewing* [1950], *Hühnerfuss and*

Garrett [1981], and *Espedal et al.* [1995]. The main chemical components of these surface films are fats, carbohydrates, proteins, sterols, and fatty acids [*Hunter and Liss,* 1981] consisting of a hydrophobic alkyl chain (preferentially with a length between C_{14} and C_{20}) and a hydrophilic head group. Typical of natural surface films are C_{16} and C_{18} components [e.g., *Hühnerfuss et al.*, 1982; *Hühnerfuss*, 1986], hence these substances were used to simulate biogenic surface films during the experiments reported herein.

SIR-C/X-SAR, mounted on board the space shuttle *Endeavour*, worked at the three radar bands L, C, and X (i.e., at radar frequencies of 1.25, 5.30, and 9.60 GHz, respectively). While the L- and C-band SARs could operate in multipolarization mode, i.e., at all polarization combinations HH, HV, VV, and VH, X-SAR was capable of taking images at vertical (VV) polarization only. The incidence angle varied between 20° and 55°, and the SAR swath width on the ground varied between 15 and 90 km. The noise floor at L and C bands was –36 and –28 dB, respectively [*Freeman et al.*, 1995], whereas at X band it depended on the incidence angle (between –40 and –30 dB for incidence angles between 25° and 55° [*Zink and Bamler,* 1995]). Thus, measured damping ratios can be affected by instrumental limitations of the SIR-C/X-SAR system (see below). For further information on the SIR-C/X-SAR system and the data quality the reader is referred to *Jordan et al.* [1995], *Zink and Bamler* [1995], and *Freeman et al.* [1995].

For the computation of the damping ratios (9) the same number of pixels from a slick-free and a slick-covered area along a scan line (width is 3 pixels, corresponding to 37.5 m) was averaged and the ratios of the obtained values were calculated. Since, in general, surface films are not homogeneous, pixels from only one scan were used for calculating the damping ratios of each radar band (instead of averaging over the whole slick-covered area). Moreover, this technique allows for better comparison of results obtained from different surface films (particularly when they are of different sizes).

3.1. Dedicated Experiments With Single Oleyl Alcohol Slicks

Oleyl alcohol (OLA, see Table 1) forms a monomolecular surface film well suited to simulate slicks of natural origin and have already been used in several surface film experiments [*Hühnerfuss et al.,* 1983a, b, 1994, 1996; *Feindt*, 1985; *Hühnerfuss,* 1986; *Okamoto et al.*, 1993; *Gade et al.*, 1998a, b; Wismann et al., submitted manuscript, 1998]. From these experiments the specific damping characteristics of this substance are well known; therefore OLA was used in both surface film experiments in Germany and Japan in order to investigate whether SIR-C/X-SAR was capable of detecting small (quasi-) biogenic surface films. For simplicity the slicks consisting of oleyl alcohol and other substances simulating natural surface films are referred to as "biogenic" surface films, instead of "quasi-biogenic." The locations of the experiments, the acquisition times of the SIR-C/X-SAR images, and the environmental conditions are listed in Table 2.

The first German experiment took place in the German Bight of the North Sea, west of the island of Sylt, on April 18, 1994 (54°54'N, 7°50'E). During this experiment, 120 L of OLA were thrown as frozen chunks from a helicopter on the sea surface. While these chunks were melting, OLA spread on the water surface such that an area of ~ 0.5 km^2 was covered by this biogenic slick. The wind speed was moderate (5 m/s), which was optimum for slick experiments. SIR-C/X-SAR images of the OLA slick, which were taken at L, C, and X band, VV polarization, are depicted in Figure 2. On the northern edge of the slick a thin "tail" was produced in order to inves-

Table 2. Time of SAR Image Acquisitions and Environmental Conditions During the Dedicated Surface Film Experiments

Date / Time, UTC	Position	Site	Substance	U_{10}, m/s	T_a, °C	SST, °C	ϑ, deg	Data Take
April 9, 2138	44°01' N, 139°55' E	J1	OLA	4.2 (338°N)	3.3	5.0	21.5	SRL 1, 8.1
April 12, 0312	43°42' N, 140°31' E	J1	OLA	9.0 (135°N)	8.0	6.2	45.0	SRL 1, 44.2
April 15, 0214	43°42' N, 140°29' E	J1	OLA	8.8 (243°N)	6.5	4.9	23.5	SRL 1, 92.2
April 16, 0153	43°17' N, 139°51' E	J1	OLA	6.8 (205°N)	7.2	5.7	31.2	SRL 1, 108.7
April 18, 0526	54°54' N, 7°50' E	G	OLA	5 (30°N)	3.3	4.8	35.6	SRL 1, 143.3
October 1, 0533	32°44' N, 135°19' E	J2	OLA	5.7 (16°N)	25.1	26.4	26.4	SRL 2, 13.3
October 2, 0515	33°49' N, 137°60' E	J2	OLA	5.2 (81°N)	23.1	23.3	47.3	SRL 2, 29.5
October 4, 0437	32°57' N, 135°05' E	J2	OLA	9.3 (84°N)	24.3	25.6	28.8	SRL 2, 61.4
October 6, 0812	54°58' N, 7°45' E	G	OLA OLME TOLG IFO 180	12 (210°N)	11.0	12	46.5	SRL 2, 96.2

The abbreviations for the test sites denote J1, northern part of the Sea of Japan; J2, Kuroshio region south of Japan; and G, German Bight of the North Sea. Also shown are the deployed substances, the wind speed U_{10} (and its direction), the air temperature T_a, the sea surface temperature SST, and the local incidence angle ϑ.

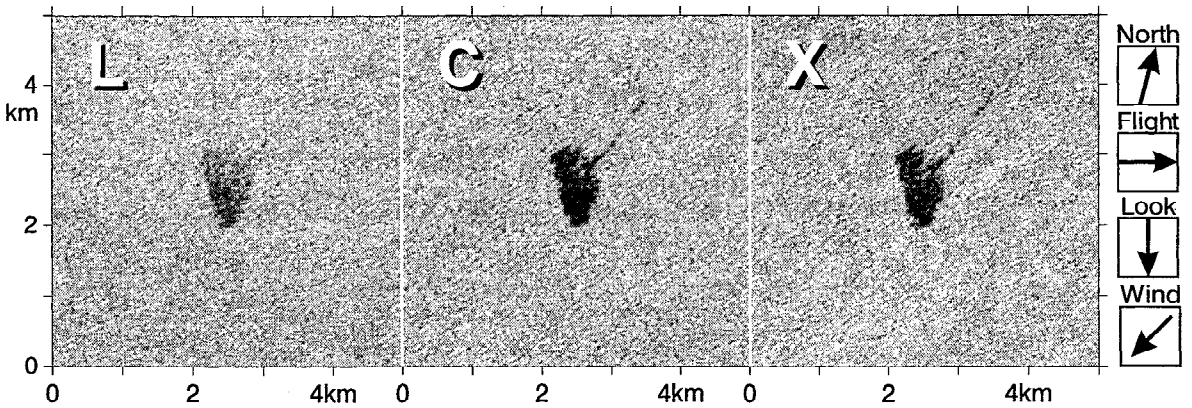

Figure 2. Spaceborne imaging radar-C/X-band synthetic aperture radar (SIR-C/X-SAR) images showing a monomolecular surface film consisting of oleyl alcohol (OLA) during the first German surface film experiment in the German Bight. The images were acquired at L, C, and X band, VV polarization, on April 18, 1994, at 0526 UTC (dimensions 5 by 5 km, images courtesy of NASA and DLR).

tigate whether SIR-C/X-SAR is capable of detecting surface slicks of small dimensions.

As an example for the reduction of the radar backscatter induced by the OLA slick a typical scan line is shown in Figure 3 (left). The corresponding (relative) backscattered power along this scan at L, C, and X band, VV polarization, is shown in Figure 3 (right). In order to allow a better discrimination the three curves are scaled in such a way that the difference of the mean radar backscatter from a slick-free water surface at adjacent radar bands is 10 dB (see the horizontal dashed lines). A distinct reduction of the radar backscatter from the slick-covered area can be delineated at all three radar bands. However, this reduction is lowest at L band (~ 5 dB), whereas it is similar at C and X band (~ 10 dB). Following *Freeman et al.* [1995] and *Zink and Bamler* [1995], the signal-to-noise ratios (SNRs) for the SAR images in this particular case are 21 (L band), 12 (C band), and 16 dB (X band). We can therefore assume that the measured reductions of the backscattered radar power, particularly at C band, are affected by instrumental limitations, i.e., by the fact that the backscattered radar power reaches the noise floor. Another manifestation of an insufficient SNR is a change of the polarization ratio on a slick-covered water surface. Following (4), the ratio of the backscattered radar power at HH and VV polarization should be independent of the slick coverage of the water surface. This has in fact been observed for L band, whereas the slick-covered water surface results in higher values of the polarization ratio at C band (these results are not shown herein, for details see *Gade* [1996]).

Figure 4 shows the damping ratios obtained from the analysis of the SIR-C/X-SAR images. From this experiment, only images at like-polarization HH and VV were received. The values for the theoretical SNR given above are inserted in Figure 4 as a dashed line. For a better discrimination between the different data points we have refrained from plotting any error bars. In all cases reported herein, however, the error of

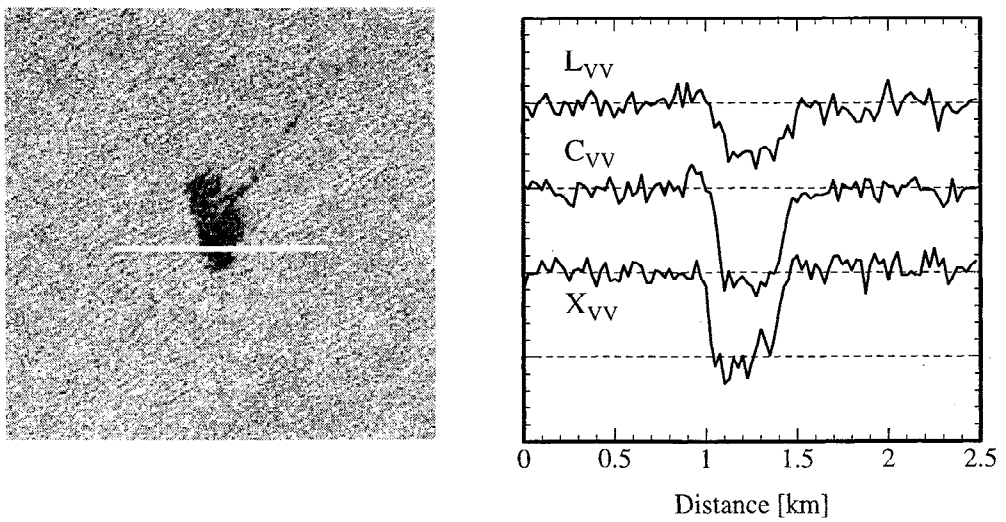

Figure 3. Scan lines through the SIR-C/X-SAR images shown in Figure 2. (left) X band, VV polarization, image with the included scan line. (right) (Relative) backscattered radar power along this scan line for all radar bands and VV polarization. The curves are scaled in such a way that the difference between the mean radar backscatter from the slick-free water surface for adjacent radar bands is 10 dB (compare the dashed horizontal lines).

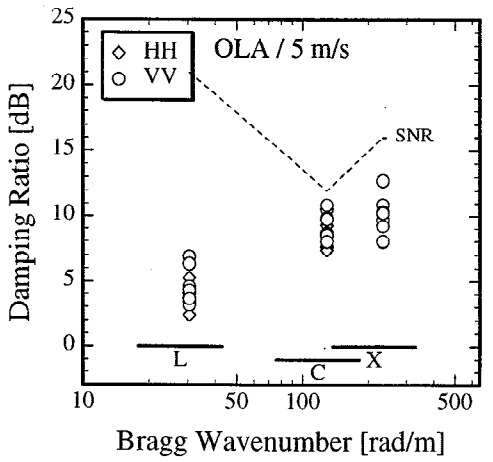

Figure 4. Damping ratios calculated from the SIR-C/X-SAR images of the OLA slick shown in Figure 2, i.e., of the first surface film experiment in the North Sea at moderate wind speed (5 m/s). The dashed line denotes the theoretical values for the signal-to-noisc ratio (SNR) for this particular data take. The horizontal bars at the bottom denote the Bragg wavenumber coverage by the different radar bands (see (1)).

the calculated data points was less than 3 dB. It can be concluded from Figure 4 that the measured damping ratios increase with Bragg wavenumber, which is in contrast to pure Marangoni damping (compare Figure 1). Furthermore, no significant dependence on the polarization was found.

A total of seven similar experiments were performed during SRL 1 and SRL 2 in the northern part of the Sea of Japan (around 44° N, 140° E) and in the Kuroshio region south of Japan (around 33° N, 136° E), respectively. In contrast to the experiments in Germany, liquid OLA was spilled from a research vessel on the water surface. Since a similar amount of surfactant was used, the slick-covered sea surface area is comparable to that of the German surface film experiment. In Figure 5, SIR-C/X-SAR images taken on April 16, 1994, at 0153 UTC are depicted at all radar bands and polarizations, showing an OLA slick (SRL 1, data take 108.7, image dimensions 5 by 5 km). As already mentioned, X-SAR was operating at VV polarization only. The analyses of the two cross-polarization images yielded the same results; therefore only HV was chosen as an example for cross polarization.

The Japanese surface film experiments were performed at different wind speeds (see Table 2), thus, the obtained results were subdivided into two wind speed ranges, i.e., into moderate (4–7 m/s) and high wind speeds (8–10 m/s). In Figure 6

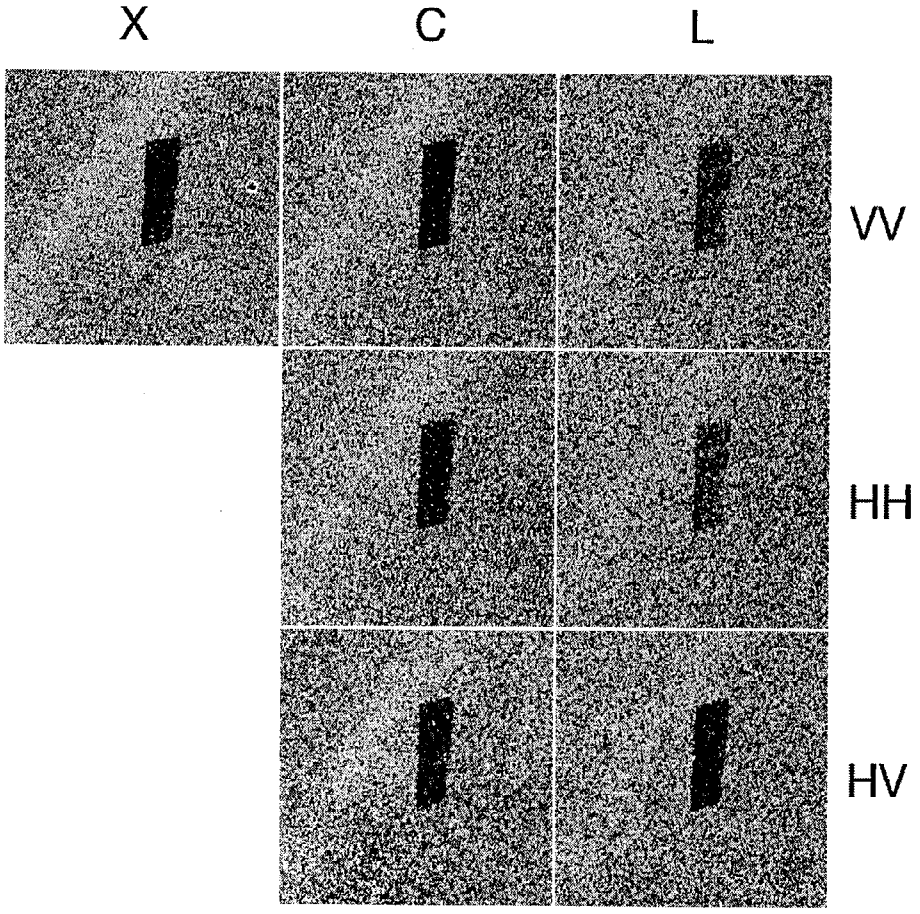

Figure 5. SIR-C/X-SAR images of an experimental OLA slick deployed during the Japanese surface film experiments in the northern part of the Sea of Japan. SAR images acquired at all radar bands (X, C, and L band) and all polarization combinations (VV, HH, and HV) are shown (images acquired on April 16, 1994, at 0153 UTC, dimensions 5 by 5 km, images courtesy of NASA and DLR).

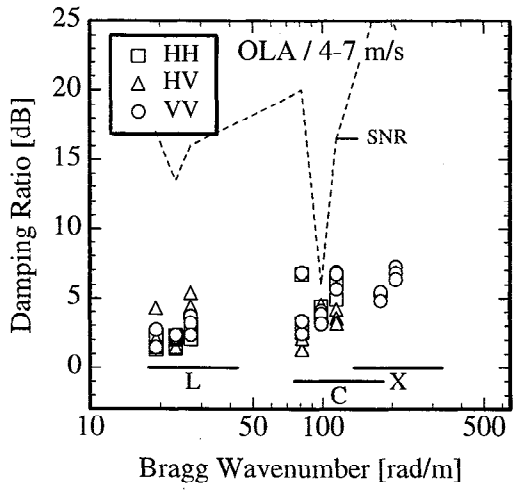

Figure 6. Damping ratios calculated from SIR-C/X-SAR images of OLA slicks acquired at moderate wind speeds (4–7 m/s) during the Japanese surface film experiments. The dashed line denotes the theoretical values for the signal-to-noise ratio (SNR). The horizontal bars at the bottom denote the Bragg wavenumber coverage by the different radar bands (see (1)).

and Figure 7 the respective data are shown. Again, we inserted the theoretical values of the SNR as dashed lines. In general, the SNR was sufficiently high for all three radar bands except for SRL 1, data take 44.2 (high wind speed), and SRL 2, data take 13.3 (low to moderate wind speed, compare Table 2). However, taking into account all results, we may assume that the observed results are not affected by instrumental limitations. Each vertically spread group of data points corresponds to one single surface film experiment (and thus one radar incidence angle). It can clearly be seen that the measured damping ratio of OLA strongly depends on wind speed; for moderate wind speed the obtained values are higher than for high wind speed, particularly at C and X band. Again, no dependence of the damping ratios on polarization was found. It is worth noting that in all cases the damping ratios for moderate wind speeds (Figure 6) are lower than those measured during the German surface film experiment (Figure 4), although deployed substance, wind speed, and radar incidence angle were similar (compare Table 2).

3.2. Dedicated Experiment With Several Different Surface Films

After successful experiments in April 1994 a larger surface film experiment was performed in the German Bight during SRL 2 on October 6, 1994. The analyses of the SAR images of the first experiment (Figure 2) showed that SIR-C/X-SAR is capable of detecting surface films of even small dimensions (see the tail at the northern edge of the slick). Therefore this time a set of (small) surface films was deployed on the sea surface, again, west of the island of Sylt (see Table 2). SIR-C/X-SAR images of the test site, which were taken at 0712 UTC on October 6, 1994, are depicted in Figure 8. In this experiment, not only artificial biogenic slicks were deployed, but also a mineral oil spill consisting of heavy fuel (technical abbreviation IFO 180). They are visible in the SAR images of Figure 8 as dark patches "a" through "g", i.e., a, IFO 180; b, OLA; c, oleic acid methyl ester (OLME); d, triolein (TOLG); e and f, TOLG and OLME, respectively, spread with the help of *n*-hexane; and g, OLME spread with the help of ethanol (for details see *Gade* [1996]). Again, the pure substances were deployed on the water surface as frozen chunks from a helicopter. The dissolved surfactants, however, had to be spilled on the water surface from a small vessel by using a long tube in order to avoid any disturbances by the ship.

Directly before the space shuttle Endeavour flew over the test site, an atmospheric front passed the area, so that the wind speed increased from 6 to 12 m/s. Under these wind conditions the various surface films are expected to show a similar damping behavior (note that the contrasts of all surface films seem to be equal at all three radar bands) and to remain on the water surface for a shorter time.

In Figure 9 the results of the SAR image analyses are shown for the four surface films which had been deployed as pure substances (IFO 180, OLA, OLME, and TOLG). In all panels the (sufficiently high) theoretical values for the SNR are included as dashed lines. The damping ratios for the slicks consisting of dissolved OLME and TOLG are similar to those for the respective pure slicks [*Gade*, 1996] and are not shown herein. Again, the damping ratios obtained at high wind speeds are relatively low with respect to those obtained at moderate wind speeds (compare Figure 4). In accordance with the other results already presented, no dependence on polarization was found for all surface films. The main result, however, from the second surface film experiment in Germany is that under high wind conditions a discrimination of different surface film materials, particularly of small natural (biogenic) slicks and (anthropogenic) oil spills, using SAR image data is not possible.

3.3. Biogenic and Anthropogenic Surface Films Imaged by Chance

The results of the German and Japanese surface film experiments demonstrate that low to moderate wind conditions are necessary to allow a discrimination between oceanic sur-

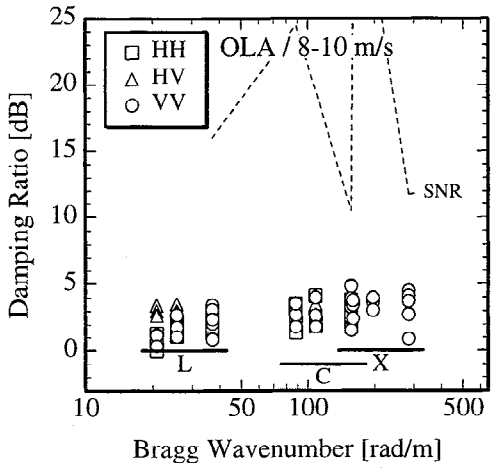

Figure 7. Damping ratios calculated from SIR-C/X-SAR images of OLA slicks acquired at high wind speeds (8–10 m/s) during the Japanese surface film experiments. The dashed line denotes the theoretical values for the signal-to-noise ratio (SNR). The horizontal bars at the bottom denote the Bragg wavenumber coverage by the different radar bands (see (1)).

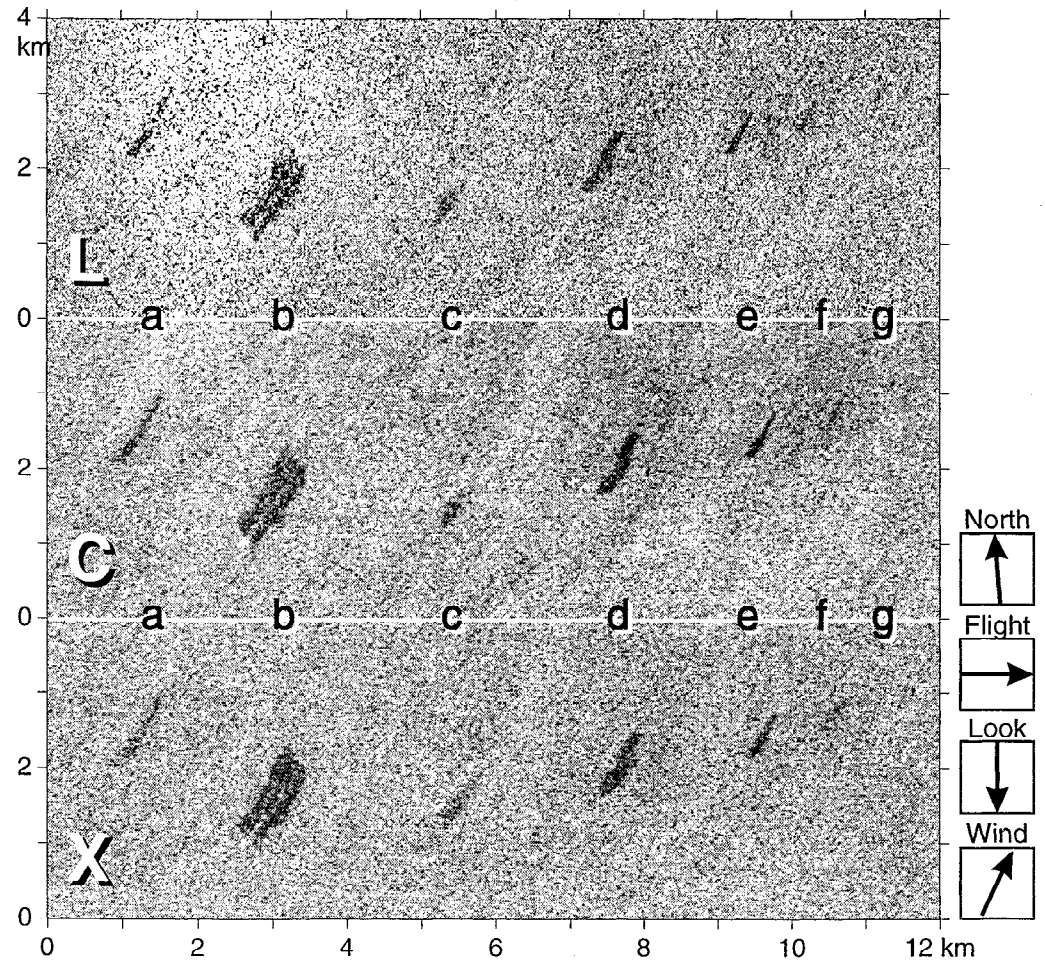

Figure 8. SIR-C/X-SAR images of the second German surface film experiment in the German Bight showing surface films consisting of a, heavy fuel (IFO 180); b, OLA; c, oleic acid methyl ester (OLME); d, triolein (TOLG); e and f, TOLG and OLME, respectively, spread with the help of *n*-hexane; and g, OLME spread with the help of ethanol. Note the bright spot at the lower end of the OLA slick, which is due to an oil surveillance ship. The images were acquired at L, C, and X band, VV polarization, on October 6, 1994, at 0712 UTC (dimensions 12 by 4 km, images courtesy of NASA and DLR).

face films of different origin (of course, different radar bands, particularly X band, are also necessary). Therefore we have analyzed SIR-C/X-SAR images of biogenic and anthropogenic surface films which were acquired during both shuttle missions in 1994 at different places of the world's oceans at low to moderate wind conditions (i.e., the estimated wind speed was lower than, say, 7 m/s). The results are presented in this section.

Figure 10 shows SIR-C/X-SAR images of biogenic surface films on a sea area west of north Denmark (56°47'N, 7°24'E) acquired on April 12, 1994, at 0728 UTC (at L, C, and X band, VV polarization). During the first shuttle mission in April 1994 an algae bloom took place in the North Sea, largely consisting of *Phaeocystis globosa*, so that at low wind speeds, large parts of the sea surface were covered by biogenic slicks. From ship observations the wind speed in this sea area was estimated to be 3–5 m/s. In order to demonstrate the different imaging of surface films by the three radar bands, certain areas are marked in Figure 10. Area "a" is a small slick which is well visible at X band (lower image) but almost invisible at L band (upper image). The small elongated slick marked as "b" is visible at all three radar bands (with the highest contrast at L band). Taking into account only the L-band image, one would classify area "c" as slick free, however, from the corresponding part of the X-band image it can be seen that there is a light coverage with surface-active material (a so-called "submonomolecular" film region). This example shows that multifrequency SAR imagery can yield important additional information about sea surface films.

In the present study, various SIR-C/X-SAR images showing biogenic surface slicks at different places of the world's oceans were analyzed. The results of these analyses are depicted in Figure 11. The large scatter of the data is due to the fact that, firstly, SAR images of different biogenic slicks (at various sea areas) were analyzed and, secondly, the natural surface films are very inhomogeneous because of different fractions of their chemical components and/or because of a different state of their development (see the results presented by *Hühnerfuss et al.* [1994, 1996]). In all cases the wind speed was low to moderate (biogenic surface slicks appear on the water surface only at low wind conditions [*Hühnerfuss and Garrett*, 1981]). For all natural surface slicks investigated herein the theoretical SNRs (see the dashed lines in Figure 11) are obviously a limit for the observed damping ratios; that is

in these cases the measurement results are strongly affected by the instrumental limitations.

The most notable characteristic of the measured damping ratios shown in Figure 11, however, is that biogenic surface films exhibit a strong damping of the long Bragg waves implying a high damping of the radar backscatter at L band. In all cases a minimum of the measured damping ratios was found at C band, i.e., at intermediate Bragg wavenumbers (however, this minimum is shallower than the scatter within a given Bragg wavenumber). This observed minimum coincides with the minimum SNR at C band (see the dashed line in Figure 11), which indicates that instrumental limitations are responsible for this peculiarity.

During the two shuttle missions, SIR-C/X-SAR images of anthropogenic mineral oil spills were also acquired. Examples of detected oil pollution are shown in Figure 12 and Figure 13. In Figure 12, SIR-C/X-SAR images are shown which were acquired over the eastern Atlantic Ocean, north of the Azores (42°49'N, 26°12'E) on April 12, 1994, at 0721 UTC, i.e., directly after sunrise (typically, oil pollution occurs during nighttime, when the polluters suppose that they are not detectable). On these images, freshly spilled mineral oil is visible as a dark narrow diagonal line. The polluting ship can be delineated as a bright spot at the western (bottom right) edge of this line. The bright area almost in the center of the C- and X-band SAR images is very likely due to heavy rain impinging on the water surface and producing small (ring) waves (a detailed description of SAR signatures of rain cells is given by *Melsheimer et al.* [this issue]). Note the low contrast of the oil spill at L band.

Another example of the imaging of oil pollution by SIR-C/X-SAR is shown in Figure 13. The large mineral oil spill visible at all three radar bands was imaged in the Baltic Sea, east of the island of Bornholm (55°02'N, 16°36'E) on April 16, 1994, at 0742 UTC. The maximum dimensions of the oil spill are 8 by 2 km, and the oil-covered surface area is ~ 15 km^2. Again, the minimum oil-induced radar contrast is observed at L band; however, at the southern edge of the spill a dark line can be seen, which may be caused by a larger thickness of the oil film. We hypothesize that the oil was discharged during the night, so that it had already been on the water surface for several hours when the images were taken.

In order to investigate the spatial dependence of the damping characteristic of the large oil spill shown in Figure 13 several scan lines parallel to the long axis of the spill were calculated. From these scan lines the damping ratios

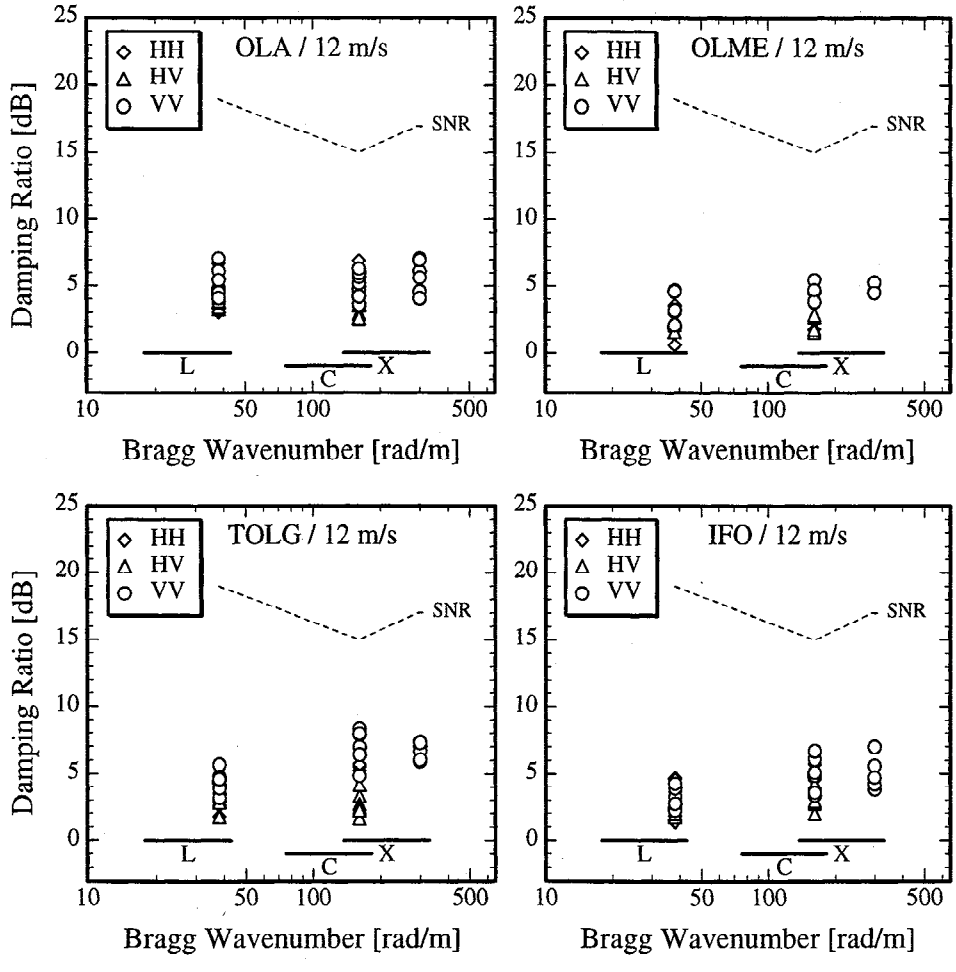

Figure 9. Damping ratios calculated from the SIR-C/X-SAR images of the IFO 180, OLA, OLME, and TOLG surface films shown in Figure 8, i.e., the four surface films spread as pure substances during the second German surface film experiment at high wind speed (12 m/s). The dashed line denotes the theoretical values for the signal-to-noise ratio (SNR) for this particular data take. The horizontal bars at the bottom of each panel denote the Bragg wavenumber coverage by the different radar bands (see (1)).

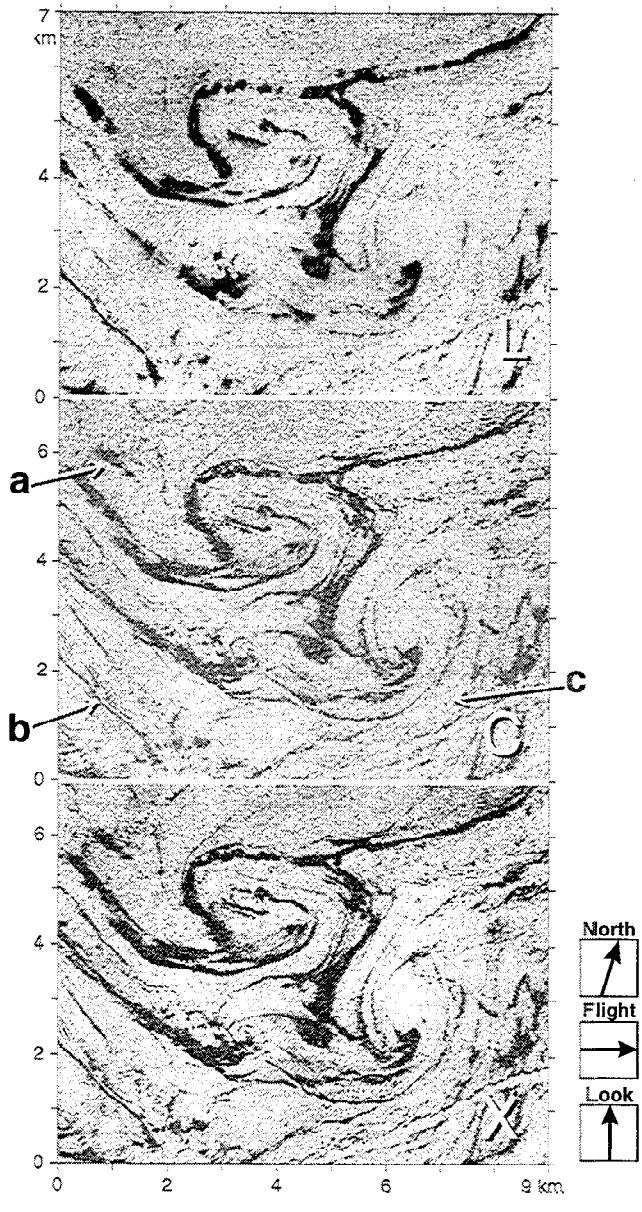

Figure 10. SIR-C/X-SAR images showing natural (biogenic) surface films in the North Sea off the coast of north Jutland (Denmark). The images were acquired at L, C, and X band, VV polarization, during the first shuttle mission on April 12, 1994, at 0728 UTC (Space Radar Laboratory (SRL) 1, data take 47.10; dimensions 9 by 7 km). For a description of the areas "a," "b," and "c," see text. Images courtesy of NASA and DLR.

shown in Figure 14 were derived. The theoretical SNR values at all radar bands are higher than 12 dB. The size of the circles corresponds to the thickness of the oil layer, assuming that this thickness is maximum at the southern edge of the spill, compare the L-band image shown in Figure 13 (according to the results of oil spill experiments presented by *Wismann et al.* [1998] the damping ratio increases with the thickness of the mineral oil spill). Most notable in Figure 14 is that for the thick part of the oil spill the increase in the damping ratios with Bragg wavenumber is linear (in the log-log space), whereas for the thin part this increase is reduced at high Bragg wavenumbers, i.e., from C to X band.

Damping ratios were calculated from the SAR images depicted in Figure 13 as well as from others showing different (not only fresh but also "weathered") oil spills, e.g., in the Persian Gulf and in the Strait of Malacca (for details, see *Gade* [1996]). From the radar backscatter from the film-free water surface as well as from ship observations the mean wind speed in the sea areas was estimated to be low to moderate (up to ~ 6 m/s) in all cases used for the present study. The results of the analyses are shown in Figure 15. Since the theoretical SNR values, on average, were better than 20 dB for all radar bands, we refrained from inserting them as a dashed line (as inserted in most of the previous figures).

The main difference to the results for biogenic surface slicks shown in Figure 11 is that the measured damping ratios for mineral oil spills are lower, particularly at L band. Furthermore, no relative minimum of the damping ratio at intermediate Bragg wavenumbers was found for (anthropogenic) mineral oil spills, but the measured damping ratios increase with Bragg wavenumber. Again, the large scatter in the data may be caused by different environmental conditions as well as different compositions and ages of the spills and hence different viscoelastic properties of the mineral oils. However, a comparison of the results of biogenic and anthropogenic surface films (Figure 11 and Figure 15, respectively) shows that there are distinct differences between the measured damping behavior.

3.4. Results of Polarimetric Studies

The multipolarization capabilities of the SIR-C radar system allowed polarimetric investigations, particularly, further insights into the scattering mechanism on the water surface. In this section the results of polarimetric studies are presented in order to investigate differences induced by the coverage of the ocean surface by a thin film of organic compounds. For the theoretical background and a survey of applications of polarimetry the reader is referred, for example, to the papers of *van Zyl et al.* [1987] and *Zebker and van Zyl* [1991].

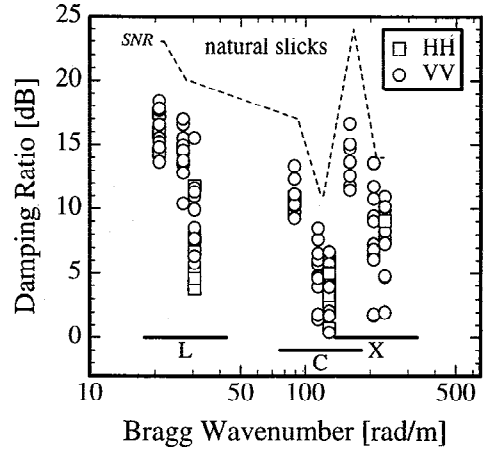

Figure 11. Damping ratios calculated from SIR-C/X-SAR images of several biogenic surface films. The SAR images were acquired during both shuttle missions in 1994 at different places of the world's oceans and at low to moderate wind speeds. The dashed line denotes the theoretical values for the signal-to-noise ratio (SNR). The horizontal bars at the bottom denote the Bragg wavenumber coverage by the different radar bands (see (1)).

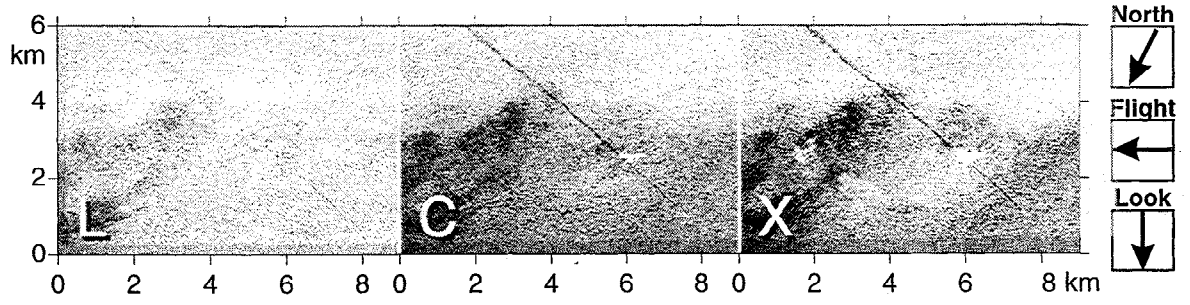

Figure 12. SIR-C/X-SAR images showing a mineral oil spill as a dark narrow diagonal line in the east Atlantic, north of the Azores. The oil-spilling ship can be delineated as a bright spot at the western end of the spill. The large bright areas visible at C and X band are due to rain cells. The images were acquired at L, C, and X band, VV polarization, during the first shuttle mission on April 12, 1994, at 0721 UTC (SRL 1, data take 47.10; dimensions 9 by 6 km, images courtesy of NASA and DLR).

Polarization signatures calculated from several SIR-C/X-SAR images showing signatures of oceanic surface films are depicted in Figure 16, Figure 17, and Figure 18. In each polarization signature the x (front) axis denotes the ellipticity angle, χ, of the electromagnetic waves ($\chi = 0°$ means zero ellipticity, i.e., linear polarization, $\chi = \pm 45°$ means circular polarization), and the y axis denotes the orientation angle, ψ ($\psi = 90°$ means vertical orientation, $\psi = 0°$ and $\psi = 180°$ mean horizontal orientation). The (vertical) z axis denotes the normalized image intensity. If the maximum image intensity is observed for VV polarization (like in the cases presented herein), the relative maximum at the front side (for $\psi = 180°$ and $\chi = 0°$) thus denotes the ratio of the radar backscatter at HH and VV polarization (polarization ratio).

Most of the SAR images of the surface film experiments around Japan (with a single OLA slick) were acquired in the multipolarization mode. As an example for our polarimetric studies, copolarization signatures calculated from the SAR images in Figure 5 are shown in Figure 16. The four polarization signatures look similar; that is, it can be delineated that for moderate wind speed (6.8 m/s) there are no significant qualitative differences observed between the backscattering, first, at L and C band (compare the upper and lower row in Figure 16) and, second, from a slick-free and a slick-covered water surface (compare the left and right column in Figure 16) at both radar bands.

Only during the second surface film experiment in the North Sea (at 12 m/s), SAR images were acquired in the multipolarization mode. Thus polarimetric studies using SAR images of different kinds of surface films under high wind conditions were performed. In Figure 17, examples of copolarization signatures are shown for a slick-free water surface as well as for a water surface covered by a (monomolecular, biogenic) TOLG slick and by heavy fuel IFO 180 (representing an anthropogenic surface film). Again, the polarization signatures are similar for the two radar bands (upper versus lower row) and for film-free and film-covered water surfaces (compare the three columns). However, the polarization signatures shown in Figure 17 qualitatively differ from those shown in Figure 16; that is, for the moderate wind speed case the maximum is more pronounced. In comparison with the other polarization signatures shown in Figure 17 we observed a higher value for the polarization ratio at L band for the TOLG-covered water surface (see the higher relative maximum at the front side).

Finally, copolarization signatures derived from SAR images of a marine surface film in the eastern Pacific are shown in Figure 18 (the SAR images are not shown herein). Although natural slicks were imaged by SIR-C/X-SAR close to this surface film, its origin could not clearly be inferred from the SAR images (i.e., from its shape and/or damping behavior). The SAR images were taken at a low incidence angle

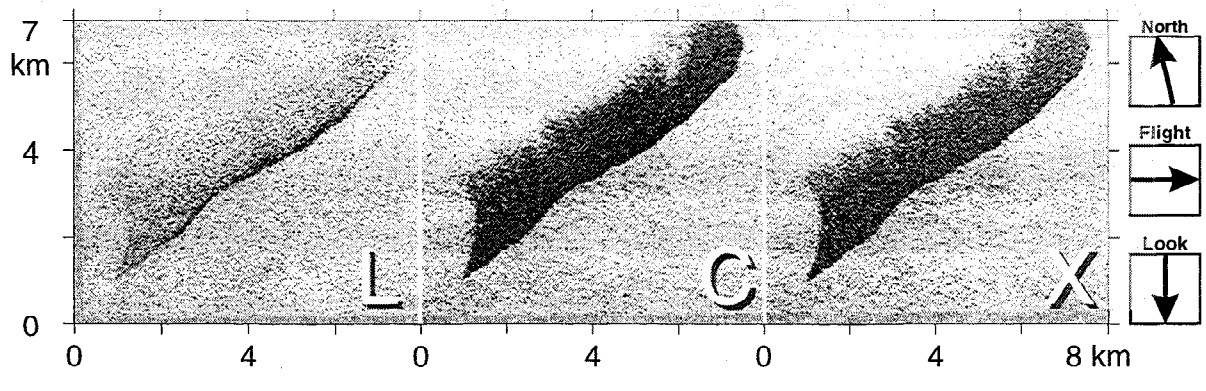

Figure 13. SIR-C/X-SAR images showing a mineral oil spill in the Baltic Sea, west of the island of Bornholm. Note the inhomogeneous contrast of the oil-covered area, particularly at L band. The images were acquired at L, C, and X band, VV polarization, during the first shuttle mission on April 16, 1994, at 0742 UTC (SRL 1, data take 112.20; dimensions 8 by 7 km, images courtesy of NASA and DLR).

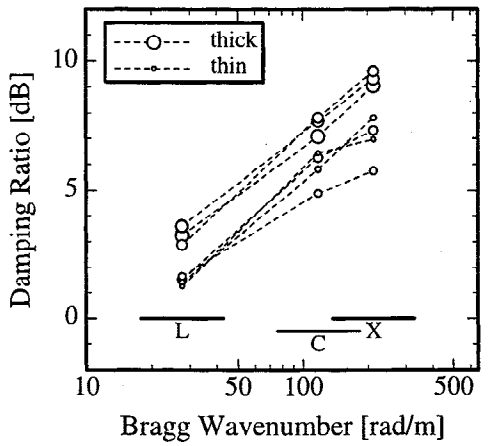

Figure 14. Damping ratios calculated from the SIR-C/X-SAR images of the mineral oil spill in the Baltic Sea shown in Figure 13. The sizes of the open circles denote the position within the slick; that is, large circles correspond to the thick (southern) edge, and small circles correspond to the thin (northern) edge. The horizontal bars at the bottom denote the Bragg wavenumber coverage by the different radar bands (see (1)).

(24.6°; SRL 1, data take 112.2) and low to moderate wind speed, and thus the calculated polarization signatures are similar to those shown in Figure 16. However, the coverage of the ocean surface with a surface film in this case leads to a pronounced change in the shape of the polarization signatures: the pedestal is higher both at L and C band.

4. Discussion

One of the goals of the experiments carried out in the German Bight of the North Sea as well as in the Sea of Japan and the Kuroshio Stream region was to investigate the influence of environmental conditions (particularly the wind speed) on the measured damping characteristic of the same substance (OLA). *Gade* [1996] discussed the differences obtained from the surface film experiments in the North Sea taking into account data which had been acquired by an airborne multifrequency/multipolarization scatterometer. He explained the changes in the damping behavior by means of the source terms of the action balance equation (6). At low wind speeds the energy input by the wind and the energy loss by wave breaking are small, so that because of the high viscous dissipation, nonlinear wave-wave interaction becomes dominant at intermediate and high Bragg wavenumbers (see (6)). At high wind speeds the reduction of wave breaking by the surface film plays an important role for the different energy flux on a film-covered water surface. Using (9) and taking into account that either the wind input (high winds) or the nonlinear wave-wave interaction (low winds) dominates, the absence of the maximum in the measured damping ratios can be explained. Furthermore, it is obvious that the absence of the damping maximum is independent of wind speed (both effects cannot be explained by Marangoni damping theory itself). The independence of the measured damping ratios on radar polarization is in accordance with Bragg scattering theory (see (4)).

A maximum damping behavior for OLA was measured during the first German surface film experiment, while in all other cases the damping ratios are smaller, even in the same wind speed range during the Japanese surface film experiments. These differences may be explained by two facts. Firstly, during the Japanese experiments, OLA was deployed on the water surface directly from a ship, whereas during the German experiments it was disseminated as frozen chunks. This may cause a different distribution of the surfactant on the water surface, i.e., a different "morphological structure," and therefore a different damping characteristic. Recently, it was shown by *Hühnerfuss et al.* [1994, 1996] that morphology effects induced, for example, by different spreading mechanisms can lead to strong changes of the damping capabilities of a monomolecular surface film. Secondly, during the first German surface film experiment the direction of the tidal flow was antiparallel to the direction of the long wave propagation. Thus the long waves should have been steeper, which, in turn, might cause a stronger wave breaking or generation of bound waves at the crests of the longer waves. The generation of bound capillary waves has first been investigated theoretically by *Longuet-Higgins* [1963]. More recently, *Ebuchi et al.* [1987, 1992] verified this theory in their experiments and showed that also small gravity-capillary waves can be bound to steep gravity waves. In wind-wave tank measurements, *Gade* [1996] and *Gade et al.* [1998c] showed that this generation mechanism can be strongly affected by the presence of a monomolecular surface film and thus can explain measured high damping ratios.

During both shuttle missions, SIR-C/X-SAR images of biogenic and anthropogenic surface films were acquired and analyzed with the aim to investigate damping characteristics of different organic film types. It can be inferred from the results shown in Figure 11 and Figure 15 that the measured damping ratios are strongly different, particularly at L band. The large damping ratios measured at low Bragg wavenumbers (L band) can be explained by means of the large sea areas which have been covered by the surface films. *Alpers and Hühnerfuss* [1989] showed that nonlinear wave-wave interaction can be responsible for a strong damping, even of waves with wavelengths longer than those which are most affected

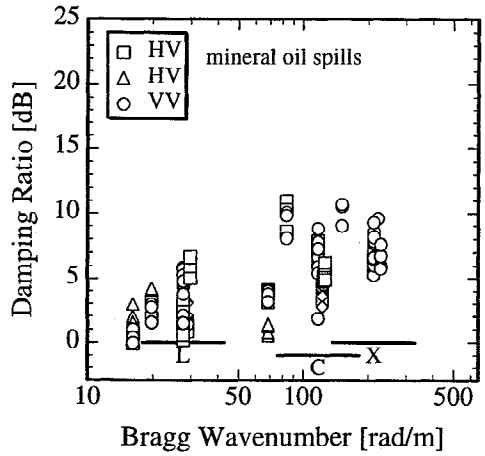

Figure 15. Damping ratios calculated from SIR-C/X-SAR images of several anthropogenic surface films, very likely consisting of mineral oil. The SAR images were acquired during both shuttle missions in 1994 at different places of the word's oceans. The horizontal bars at the bottom denote the Bragg wavenumber coverage by the different radar bands (see (1)).

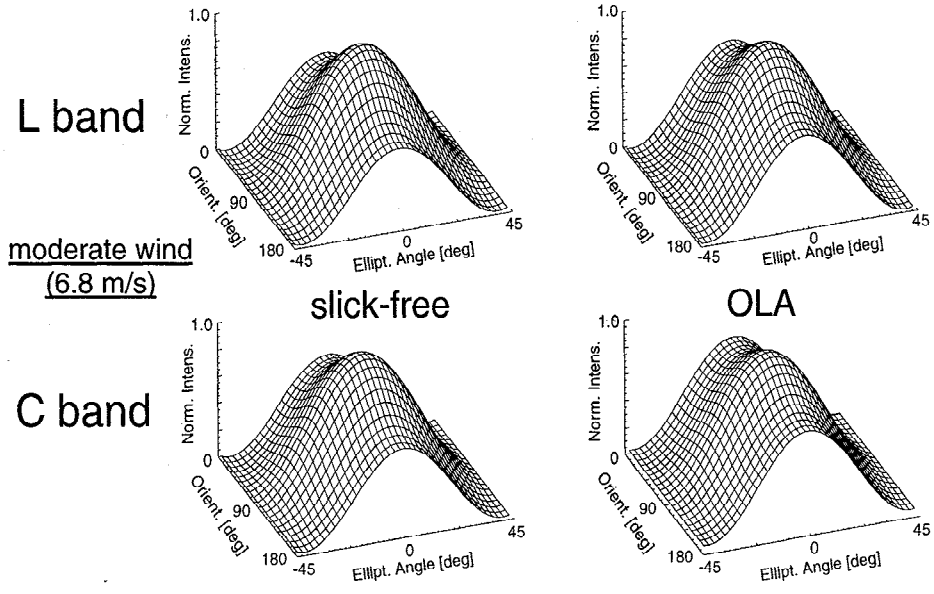

Figure 16. Polarization signatures calculated from SAR images of the OLA slick shown in Figure 5 for (left) a slick-free water surface and (right) a water surface covered with OLA (data take 108.7). During this surface film experiment with an oleyl alcohol slick the wind conditions were moderate (6.8 m/s). The upper two signatures were calculated from the L-band SAR images, and the lower two signatures were calculated from the C-band SAR images. The x-, y-, and z-axes denote ellipticity angle, orientation angle, and normalized intensity of the microwaves (see text).

by Marangoni damping (compare Figure 1). However, mineral oil spills typically cover a small sea area, so that the energy transfer by nonlinear wave-wave interaction is less, and thus lower damping ratios at L band are measured.

The L-band damping ratios derived from SAR images of natural biogenic surface films are higher than those derived from SAR images of the artificial OLA slicks (compare Figure 11 as well as Figure 4, Figure 6, and Figure 7). This result may be due to a larger fraction of biogenic substances of strong damping capabilities within the natural surface films. Recently, *Hühnerfuss et al.* [1996] showed that the damping behavior of natural biogenic surface films could successfully be simulated by a quasi-biogenic slick consisting of palmitic acid methyl ester (PME), which had been deployed with the help of spreading solvents (PME exhibits a stronger damping characteristic than OLA).

In the damping curves of biogenic surface films a typical minimum at intermediate Bragg wavenumbers (C band) was

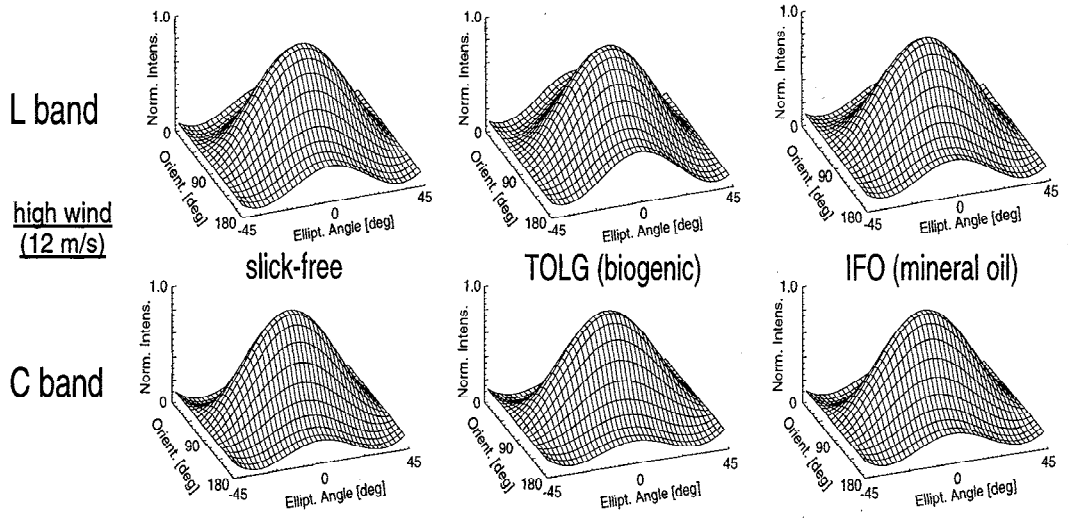

Figure 17. Polarization signatures calculated from SAR images of the second German surface film experiment shown in Figure 8 for (left) a slick-free water surface and a water surface covered with (middle) a monomolecular TOLG slick and (right) a mineral oil spill (IFO). During this surface film experiment the wind conditions were high (12 m/s). The upper signatures were calculated from the L-band SAR images, and the lower signatures were calculated from the C-band SAR images. The x-, y-, and z-axes denote ellipticity angle, orientation angle, and normalized intensity of the microwaves (see text).

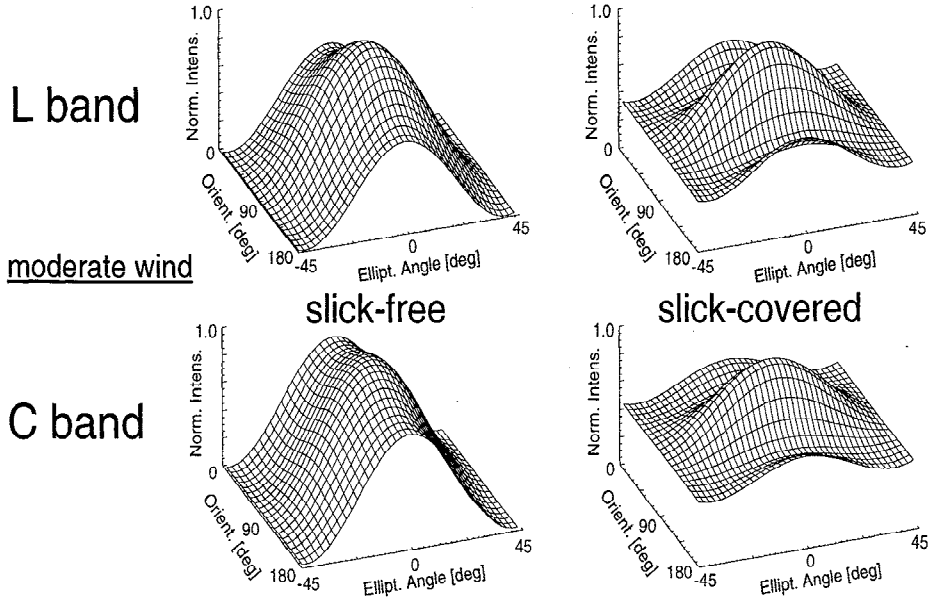

Figure 18. Polarization signatures calculated from SAR images of marine surface films in the Eastern Pacific Ocean, off the Mexican coast for (left) a slick-free and (right) a slick-covered water surface. From the SAR image (not shown herein), low to moderate wind conditions can be inferred (up to ~ 7 m/s). The upper two signatures were calculated from the L-band SAR images and the lower two signatures from the C-band SAR images. The *x*-, *y*-, and *z*-axes denote ellipticity angle, orientation angle, and normalized intensity of the microwaves (see text).

found. This minimum coincides with a corresponding minimum (theoretical) SNR at C band. Biogenic surface films exhibit very strong damping characteristics over the whole Bragg wavenumber range (which have already been measured using an airborne scatterometer [*Hühnerfuss et al.*, 1996]). Therefore the observed minima are very likely caused by instrumental limitations of the SAR system; that is, the signal-to-noise ratio of SIR-C/X-SAR is too low for measuring high damping ratios, even at low wind speeds. In the case of natural slicks covering large sea areas, surfactants are known to prevail not only within the slicks, but also in the surface areas between [*Hühnerfuss et al.*, 1977; *Espedal et al.*, 1995]. Therefore low C-band damping ratios may also be due to a reduced contrast of the damping behavior of the slick-covered and slick-free surface areas. Results from airborne SAR measurements (which are comparable to the damping ratios measured by SIR-C/X-SAR (P. Fischer, personal communication, 1996)) are expected to give further insights into this problem.

The results presented herein are in agreement with those presented by *Neville et al.* [1984], who also found lower damping ratios at L band than at X band from their SAR images of marine oil spills. It should further be stressed that the damping ratios of biogenic and anthropogenic surface films are comparable at C band, which unfortunately is the radar band of the ERS–1 and ERS–2 SARs.

In Figure 16, Figure 17, and Figure 18, L- and C-band co-polarization signatures are shown, which were calculated from SIR-C SAR images of different marine surface films. The aim of these studies was to find out whether or not any differences in the polarization signatures may help to discriminate between different kinds of surface films.

In Figure 16, all polarization signatures show large values of the polarization ratio (i.e., the relative maximum at their front side). Assuming radar backscattering from a slightly roughened ocean surface (Bragg scattering), these values should be smaller (see the examples shown by *Zebker and van Zyl* [1991]). This implies that Bragg scattering is not the only backscattering mechanism and that specular reflection also gives an impact on the backscattered radar signal at small incidence angles (lower than 30°). This can also explain the relatively small damping ratios obtained from the SAR images of the Japanese surface film experiments, however, low damping measured at higher incidence angles cannot be explained yet.

The shape of the polarization signatures shown in Figure 17 is typical of radar backscattering from a rough surface. Therefore, following the above argument, it can be inferred that Bragg scattering dominates the radar backscattering at intermediate incidence angles (here 46.5°). As for the calculated damping ratios, a discrimination between the different surface films, particularly between the biogenic slicks and the mineral oil spill, is not possible for high wind conditions using polarimetric studies.

The polarization signatures obtained from SAR images which were acquired at low incidence angles (lower than 30°, Figure 16 and Figure 18) are similar for a slick-free water surface. Again, we delineate from these results that specular reflection plays an important role at low incidence angles. However, for a film-covered water surface significant differences have been observed, which may be due to the lower wind speed in the case of the surface film detected in the eastern Pacific (see Figure 18; the wind speed is estimated to be lower than 5 m/s). It can be inferred from Figure 18 and from the other results discussed herein that, firstly, the fraction of specular backscattering in this case is higher at C band than at L band and, secondly, that from a slick-covered water surface the backscattered radar signal reaches the noise floor both at L and C band, which results in an increase in the pedestals. The latter result can explain that the analyses of SAR images of

biogenic surface films yields lower damping ratios at C band than those measured by a scatterometer [*Hühnerfuss et al.*, 1996]. However, assuming a very thick oil film, multireflection of the radar beam within the oil layer may also lead to an increase in the pedestal and can therefore also explain the observed differences in the polarization signatures.

5. Conclusions

During the two SIR-C/X-SAR missions in 1994, various surface film experiments were performed in order to investigate whether or not SIR-C/X-SAR is capable of discriminating between biogenic and anthropogenic oceanic surface films. For this purpose a well-defined surface-active substance, oleyl alcohol (OLA), was deployed on the ocean surface under different environmental conditions, particularly different wind speeds. We found that the measured damping ratios, i.e., the ratios of the backscattered radar power from a slick-free and a slick-covered water surface, at L, C, and X band strongly depend on the wind, that is, they decrease with increasing wind speed. This effect may be explained by means of the source terms of the spectral action, i.e., by the influence of the surface film on wind input, wave breaking, and nonlinear wave-wave interaction.

The different damping behavior of OLA measured at moderate wind speeds (~ 5 m/s) during the surface film experiments in the North Sea and around Japan may be caused by the different deploying techniques during the experiments and thus by a different morphology of the OLA film resulting in different damping capabilities. However, the influence of the surface film on the generation of bound Bragg waves by steep gravity waves may also explain higher damping ratios which were observed during the German experiment. Moreover, the radar look direction relative to the wind direction was different during the various surface film experiments (e.g., the SAR was looking approximately downwind and almost upwind during the first and second German surface film experiments, respectively). Parallel to the shuttle overflights, radar backscatter measurements with an airborne scatterometer were carried out in the German Bight during both shuttle missions [*Gade et al.*, 1998b]. The results of these measurements give rise to the conclusion that the damping ratios are independent of radar look direction relative to the wind direction (i.e., on the azimuth angle), which was explained by *Gade et al.* [1998b] by two different effects: first, by the isotropy of the viscous damping (both on a slick-free and a slick-covered water surface) and second, by the fact that the influence of the slick coverage on the other source terms (like the energy input by the wind) may not depend on the azimuth angle. If these source terms dominate in (9), the measured damping ratios have to be independent of antenna look direction.

Furthermore, several SIR-C/X-SAR images of various biogenic and anthropogenic surface films at different places of the world's oceans were analyzed. It was shown that biogenic (natural) surface slicks cause a strong damping at L band, whereas anthropogenic (mineral) oil spills cause only low L-band damping ratios. At C and X band the observed damping ratios are similar, which, particularly at C band, is obviously due to an insufficient signal-to-noise ratio of the SIR-C/X-SAR system (see the dashed lines inserted into the figures). The presented results, however, show that multifrequency SAR imagery yields more reliable information about the damping characteristics of oceanic surface films, which, in turn, is needed for a better discrimination between different kinds of surface films, particularly under low to moderate wind conditions.

Polarimetric studies were performed using multipolarization L- and C-band SAR images of various oceanic surface films. It was found that the copolarization signatures for film-free and film-covered water surfaces are similar in most cases and for both radar bands. However, a significant change of the shape of the polarization signatures caused by the presence of a marine surface film was observed for SAR images acquired over the eastern Pacific. This change may be due to a high noise portion; that is, the SNR is too low, and the radar signal from a film-covered water surface may reach the noise floor. It can be concluded from the polarimetric studies that these analyses are less useful for the discrimination of biogenic and anthropogenic marine surface films. Nevertheless, the obtained information about the scattering mechanism is useful for the interpretation of the observed data.

Summarizing, we have shown that multifrequency/multipolarization SAR imagery is advantageous for detection of oceanic surface films; that is, important additional information can be inferred from these SAR data. The evidence shows that under low to moderate wind conditions, multifrequency radar techniques are capable of discriminating between the different kinds of surface films (particularly in combination with improved slick detection algorithms), whereas at high wind conditions a discrimination (on a basis of damping measurements) is impossible.

Acknowledgments. The authors would like to thank H. Runge at DLR and B. Holt at JPL for helping us to find and to get some of the SAR images. We are grateful to M. Keßler, M. Kim, G. Tanck, and S. Ufermann for their engaged help in processing the SAR data. This work has been supported by the German Space Agency (DARA) under contract 01QS9016 / 50QS90165 and by the German Science Foundation (DFG) under contract Hu583/1-2.

References

Alpers, W., and H. Hühnerfuss, Radar signatures of oil films floating on the sea and the Marangoni effect, *J. Geophys. Res., 93,* 3642–3648, 1988.

Alpers, W., and H. Hühnerfuss, The damping of ocean waves by surface films: A new look at an old problem, *J. Geophys. Res., 94,* 6251–6265, 1989.

Cini, R., and P.P. Lombardini, Damping effect of monolayers on surface wave motion in a liquid, *J. Colloid Interface Sci., 65,* 387–389, 1978.

Cini, R., P.P. Lombardini, and H. Hühnerfuss, Remote sensing of marine slicks utilizing their influence on wave spectra, *Int. J. Remote Sens., 4,* 101–110, 1983.

Dietz, R.S., and E.C. Lafond, Natural slicks on the ocean, *J. Mar. Res., 9,* 69–76, 1950.

Ebuchi, N., H. Kawamura, and Y. Toba, Fine structure of laboratory wind-wave surfaces studied using an optical method, *Boundary Layer Meteorol., 39,* 133–151, 1987.

Ebuchi, N., H. Kawamura, and Y. Toba, Statistical properties of microwave backscattering from laboratory wind wave surfaces, *J. Oceanogr., 48,* 139–154, 1992.

Ermakov, S.A., E.M. Zujkova, A.R. Panchenko, S.G. Salashin, T.G. Talipova, and V.I. Titov, Surface film effect on short wind waves, *Dyn. Atmos. Oceans, 10,* 31–50, 1986.

Espedal, H.A., O.M. Johannessen, and J. Knulst, Natural films in coastal waters, in *Proceedings of IGARSS'95, Florence, Italy,* pp. 2106–2108, IEEE, Piscataway, NJ, 1995.

Ewing, G., Slicks, surface films and internal waves, *J. Mar. Res., 9,* 161–187, 1950.

Feindt, F., Radar-Rückstreuexperimente am Wind-Wellen-Kanal bei sauberer und filmbedeckter Wasseroberfläche im X band (9.8 GHz), Dissertation, *Fachbereich 15* (Geowiss.), Univ. Hamburg, Hamburg, Germany, 224 pp., 1985.

Freeman, A., M. Alves, B. Chapman, J. Cruz, Y. Kim, S. Shaffer, J.

Sun, E. Turner, and K. Sarabandi, SIR-C data quality and calibration results, *IEEE Trans. Geosci. Remote Sens., 33,* 848–857, 1995.

Frysinger, G.S., W.E. Asher, G.M. Korenowski, W.R. Barger, M.A. Klusty, N.M. Frey, and R.K. Nelson, Study of ocean slicks by nonlinear laser processes, 1, Second-harmonic generation, *J. Geophys. Res., 97,* 5253–5269, 1992.

Gade, M., Untersuchungen zur Abbildung biogener und anthropogener Oberflächenfilme auf dem Meer mit Hilfe von Radarsensoren, Dissertation, *Fachbereich 15* (Geowiss.), 170 pp., Univ. Hamburg, Hamburg, Germany, 1996.

Gade, M., W. Alpers, H. Hühnerfuss, and P.A. Lange, Wind wave tank measurements of wave damping and radar cross sections in the presence of monomolecular surface films, *J. Geophys. Res., 103,* 3167–3178, 1998a.

Gade, M., W. Alpers, H. Hühnerfuss, V.R. Wismann, and P.A. Lange, On the reduction of the radar backscatter by oceanic surface films: scatterometer measurements and their theoretical interpretation, *Remote Sens. Environ.,* in press, 1998b.

Gade, M., W. Alpers, S.A. Ermakov, H. Hühnerfuss, and P.A. Lange, Wind wave tank measurements of bound and freely propagating short gravity-capillary waves, *J. Geophys. Res.,* in press, 1998c.

Garrett, W.D., Damping of capillary waves at the air-sea interface by oceanic surface-active material, *J. Mar. Res., 25,* 279–291, 1967.

Hasselmann, K., Grundgleichungen der Seegangsvorhersage, *Schiffstechnol. Z.,* 1, 191–195, 1960.

Hühnerfuss, H., The molecular structure of the system water/monomolecular surface film and its influence on water wave damping, Habilitationsschr., *Fachbereich 13* (Chem.), 245 pp., Univ. Hamburg, Hamburg, Germany, 1986.

Hühnerfuss, H., and W. D. Garrett, Experimental sea slicks: Their practical applications and utilization for basic studies of air-sea interactions, *J. Geophys. Res., 86,* 439–447, 1981.

Hühnerfuss, H., W. Walter, and G. Kruspe, On the variability of surface tension with mean wind speed, *J. Phys. Oceanogr., 7,* 567–571, 1977.

Hühnerfuss, H., P.A. Lange, and W. Walter, Wave damping by monomolecular surface films and their chemical structure, I, Variation of the hydrophobic part of carboxylic acid esters, *J. Mar. Res., 40,* 209–225, 1982.

Hühnerfuss, H., W. Alpers, A. Cross, W. D. Garrett, W. C. Keller, P. A. Lange, W. J. Plant, F. Schlude, and D. L. Schuler, The modification of X and L band radar signals by monomolecular sea slicks, *J. Geophys. Res., 88,* 9817–9822, 1983a.

Hühnerfuss, H., W. Alpers, W. D. Garrett, P. A. Lange, and S. Stolte, Attenuation of capillary and gravity waves at sea by monomolecular organic surface films, *J. Geophys. Res., 88,* 9809–9816, 1983b.

Hühnerfuss, H., A. Gericke, W. Alpers, R. Theis, V. Wismann, and P.A. Lange, Classification of sea slicks by multi-frequency radar techniques: New chemical insights and their geophysical implications, *J. Geophys. Res., 99,* 9835–9845, 1994.

Hühnerfuss, H., W. Alpers, H. Dannhauer, M. Gade, P.A. Lange, V. Neumann, and V. Wismann, Natural and man-made sea slicks in the North Sea investigated by a helicopter-borne 5-frequency radar scatterometer, *Int. J. Remote Sens., 17,* 1567–1582, 1996.

Hunter, K.A., and P.S. Liss, Organic sea surface films, in *Marine Organic Chemistry: Evolution, Composition, Interactions and Chemistry of Organic Matter in Sea Water,* edited by E.K. Duursma and R. Dawson, pp. 259–298, Elsevier, New York, 1981.

Jordan, R.L., B.L. Honeycutt, and M. Werner, The SIR-C/X-SAR synthetic aperture radar system, *IEEE Trans. Geosci. Remote Sens., 33,* 829–839, 1995.

Lange, P.A. and H. Hühnerfuss, Drift response of monomolecular slicks to wave and wind action, *J. Phys. Oceanogr., 8,* 142–150, 1978.

Lange, P.A. and H. Hühnerfuss, Horizontal surface tension gradients induced in monolayers by gravity water wave action, *J. Phys. Oceanogr., 14,* 1620–1628, 1984.

Lombardini, P.P., B. Fiscella, P. Trivero, C. Cappa, and W.D. Garrett, Modulation of the spectra of short gravity waves by sea surface films: slick detection and characterization with a microwave probe, *J. Atmos. Oceanic. Technol., 6,* 883–890, 1989.

Longuet-Higgins, M.S., The generation of capillary waves by steep gravity waves, *J. Fluid Mech., 52,* 725–751, 1963.

Lucassen, J., Effect of surface-active material on the damping of gravity waves: A reappraisal, *J. Colloid Interface Sci., 85,* 52–58, 1982.

Lucassen-Reynders, E.H., and J. Lucassen, Properties of capillary waves, *Adv. Colloid Interface Sci., 2,* 347–395, 1969.

Melsheimer, C., W. Alpers, and M. Gade, Investigation of multifrequency/multipolarization radar signatures of rain cells over the ocean using SIR-C/X-SAR data, *J. Geophys. Res.,* this issue.

Mitsuyasu, H., and T. Honda, Wind-induced growth of water waves, *J. Fluid Mech., 123,* 425–442, 1982.

Neville, R.A., V. Thomson, L. Gray, and R.K. Hawkins, Observation of two test oil spills with a microwave scatterometer and a synthetic aperture radar, in *Remote Sensing for the Control of Marine Pollution,* edited by J.M. Massin, pp. 257–266, Plenum, New York, 1984.

Okamoto, K., H. Masuko, S. Ochiai, S. Uratsuka, K. Nakamura, H. Horie, M. Fujita, M. Shimada, M. Nakai, and A. Shibata, Artificial oil pollution detection and wave observation in the sea adjacent to Japan by ERS-1 SAR, *Proceedings of the First ERS-1 Symposium - Space at the Service of Our Environment, Cannes, France,* ESA Publ. Dev., Nordwijk, The Netherlands, 1993.

Onstott, R., and C. Rufenach, Shipboard active and passive microwave measurement of ocean surface slicks off the southern California coast, *J. Geophys. Res., 97,* 5315–5323, 1992.

Pellemans, A.H.J.M, W.G. Bos, H. Konongs, and R.W. van Swol, Oil spill detection on the North Sea using ERS–1 SAR data, *BCRS Rep. 94–30,* Neth. Remote Sens. Board, Delft, The Netherlands, 1995.

Phillips, O.M., Spectral and statistical properties of the equilibrium range in wind-generated gravity waves, *J. Fluid Mech., 156,* 505–531, 1985.

Plant, W.J., A relationship between wind stress and wave slope, *J. Geophys. Res., 87,* 1961–1967, 1982.

Sloggett, D.R. and I.S. Jory, An operational, satellite-based, European oil slick monitoring system, in *Sensors and Environmental Applications of Remote Sensing*, edited by J. Askne, pp. 183–187, Balkema, Brookfield, Vt., 1995.

Tang, S., and J. Wu, Suppression of wind-generated ripples by natural films: A laboratory study, *J. Geophys. Res., 97,* 5301–5306, 1992.

Valenzuela, G.R., Theories for the interaction of electromagnetic and oceanic waves - A review, *Boundary Layer Meteorol., 13,* 61–85, 1978.

van Zyl, JJ, H.A. Zebker, and C. Elachi, Imaging radar polarization signatures: Theory and observations, *Radio Sci., 22,* 529–543, 1987.

Wahl, T., T. Anderssen, and Å. Skøelv, Oil spill detection using satellite based SAR: Pilot operation phase, final rep., Norw. Def. Res. Estab., Kjeller, Norway, 1994.

Wei, Y., and J. Wu, In situ measurements of surface tension, wave damping, and wind properties modified by natural films, *J. Geophys. Res., 97,* 5307–5313, 1992.

Wismann, V., M. Gade, W. Alpers, and H. Hühnerfuss, Radar signatures of marine mineral oil spills measured by an airborne multi-frequency radar, *Int. J. Rem. Sens.*, in press, 1998.

Wright, J.W., A new model for sea clutter, *IEEE Trans. Antennas Propag., AP-16,* 217–223, 1968.

Wu, J., Suppression of oceanic ripples by surfactant-spectral effects deduced from sun-glitter, wave-staff and microwave measurements, *J. Phys. Oceanogr., 19,* 238–245, 1989.

Zebker, H.A., and J.J. van Zyl, Imaging radar polarimetry: A review, *Proc. IEEE, 79,* 1583–1606, 1991.

Zink, M., and R. Bamler, X-SAR radiometric calibration and data quality, *IEEE Trans. Geosci. Remote Sens., 33,* 840–847, 1995.

W. Alpers and M. Gade, Institut für Meereskunde, Universität Hamburg, Troplowitzstraße 7, D-22529 Hamburg, Germany. (e-mail: alpers@ifm.uni-hamburg.de; gade@ifm.uni-hamburg.de)

H. Hühnerfuss, Institut für Organische Chemie, Universität Hamburg, Martin-Luther-King-Platz 6, D-20146 Hamburg, Germany (e-mail: huehnerf@chemie.uni-hamburg.de).

T. Koboyashi and H. Masuko, Communication Research Laboratory, 4-2-1 Nukui-kita-machi, Koganei, Tokyo 184, Japan. (e-mail: tkoba@crl.co.jp; masuko@crl.co.jp)

(Received September 11, 1996, revised June 9, 1997; accepted July 3, 1997.)